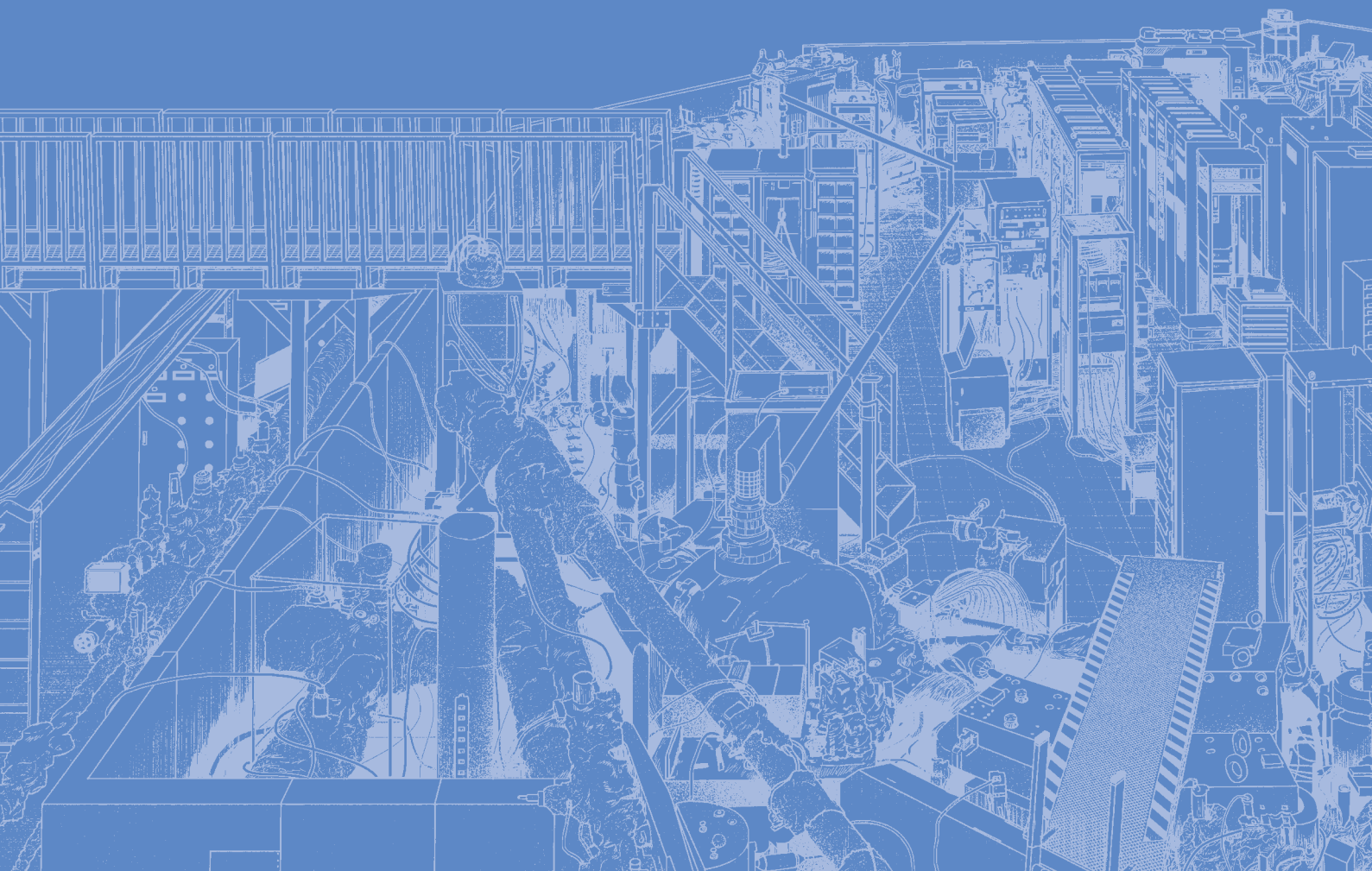
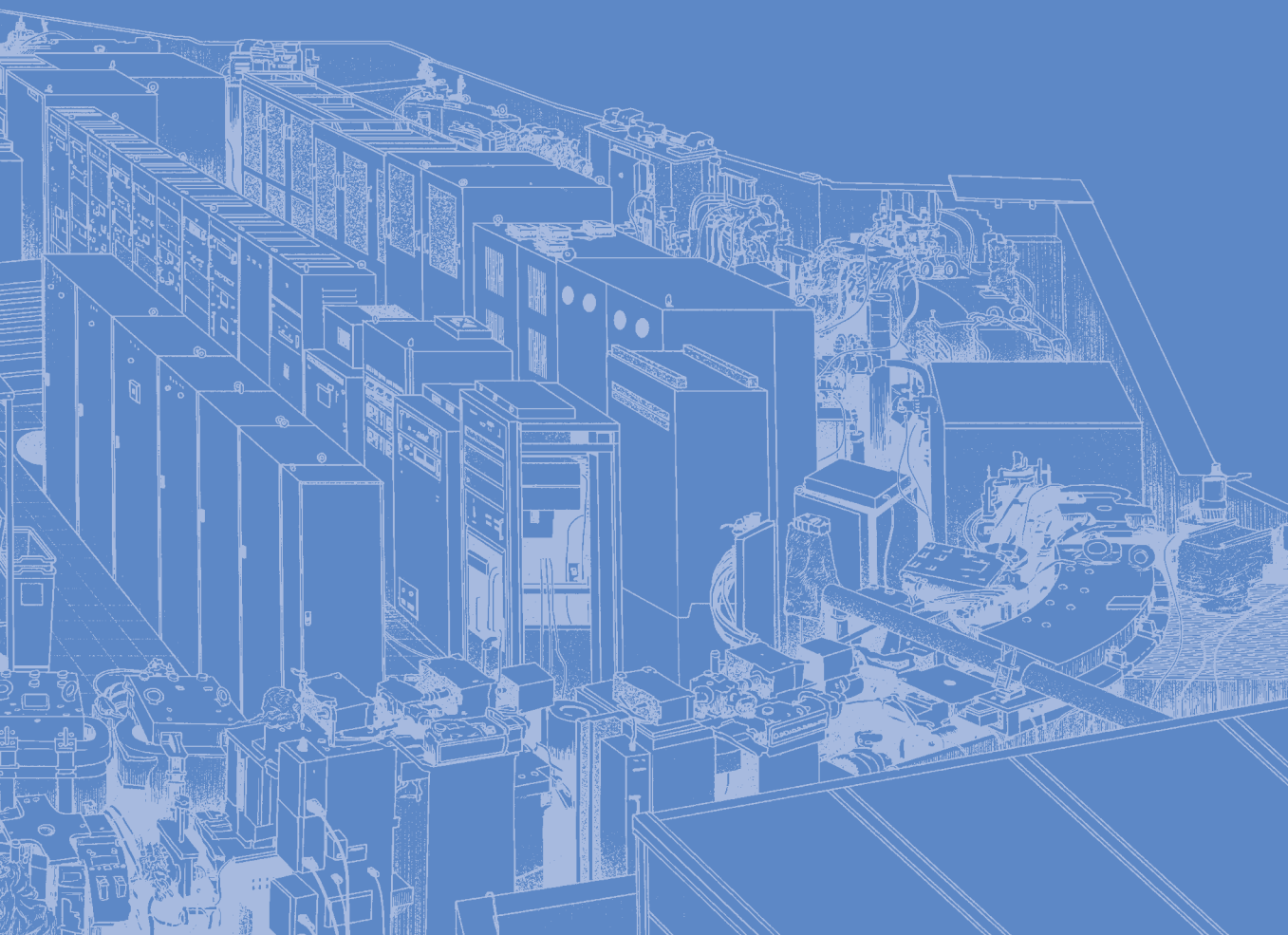


# III-3

Chemistry





BL4B

## Ligand Field in Fe-based spin-crossover Coordination Polymer Revealed by Soft x-ray Absorption Spectroscopy

K. Yamagami

Japan Synchrotron Radiation Research Institute (JASRI), 1-1-1, Sayo-cho, Sayo-gun, Hyogo 679-5198, Japan

The 3d transition metal elements have many attractive physical phenomena in solid-state materials such as unconventional superconductivity, metal-insulator transition, and spin transition involving magnetism due to their high charge, spin, and orbital degrees of freedom. Since the 3d electronic states in solids are controlled by “ligand field effects” due to the type and symmetry of ligands and “charge transfer interactions” between transition metal ions via ligands, experimental exploration of element-specific electronic states provides fundamental information for understanding macroscopic properties involving 3d electrons.

In this study, I focus on “spin crossover,” which is strongly related to ligand field effects and spin degrees of freedom. Spin crossover is a phenomenon in which a change in the splitting width of the 3d orbital level causes an electron spin transition. In particular, the spin crossover transition that appears in transition metal coordination polymers exhibits thermal hysteresis. Since the transition temperature and the shape of the hysteresis depend on the guest molecules encapsulated in the coordination polymer, it is attracting attention as a new adsorption material along with activated carbon and silica gel. However, spectroscopic element-specific analysis of the 3d orbital levels associated with thermal spin-crossover transitions in coordination polymers is challenging due to their low chemical stability against light source irradiation.

In this work, I performed the soft x-ray absorption spectroscopy (XAS) for the Fe-based spin-crossover coordination polymer  $\text{Fe}(\text{pyrazine})_2[\text{Pt}(\text{CN})_4]$  to investigate the contribution of ligand field effect for  $\text{Fe}^{2+}$  ions under the tetragonal symmetry related to the thermal spin crossover transition.

The XAS measurement was done at UVSOR BL4B. The Fe  $L_{2,3}$ -edge XAS spectra was recorded by the total electron yield (TEY) and partial fluorescence yield (PFY) modes obtained by the drain current for TEY and SDD detector for PFY, respectively. The powder samples were thinly expanded on the carbon tape and its temperature was controlled by the liq.  $\text{N}_2$  and ceramic heaters. During measurement, the x-ray irradiated damage of the samples was checked from the position and irradiation time dependence of the XAS spectra. The energy calibration was done by the Fe  $L_{2,3}$ -edge XAS spectra of  $\text{Fe}_3\text{O}_4$ . All XAS spectra were normalized by the incoming x-ray flux.

In this report, I show the XAS results in PFY mode since the huge noise was observed in TEY mode. Fig. 1 shows the temperature dependent Fe  $L_{2,3}$ -edge XAS spectra. During one cycle of temperature change, I

observed a spectral change corresponding to the transition between the high-spin (HS) state at high-temperature and the low-spin (LS) state at low-temperature and found that the transition temperature differs between the heating and the cooling processes. According to the simplest  $\text{Fe}^{2+}$  ionic model calculations, the  $\text{Fe}^{2+}$  ions have only HS state at 320 K and only LS state at 240 K. Therefore, I carried out the linear fitting analysis by the spectra at 320 K and 240 K to estimate the spin state weight around spin-crossover transition. The fitting results reproduce the experimental spectra and plotted as the function of the temperature together with the macroscopic magnetometry result of  $\text{Fe}(\text{pyrazine})_2[\text{Pt}(\text{CN})_4]$  (Fig. 2). I found that the transition temperature between XAS spectra and magnetization is quite different, seemingly linking to the different thermal stability between the electronic state and structural distortion.

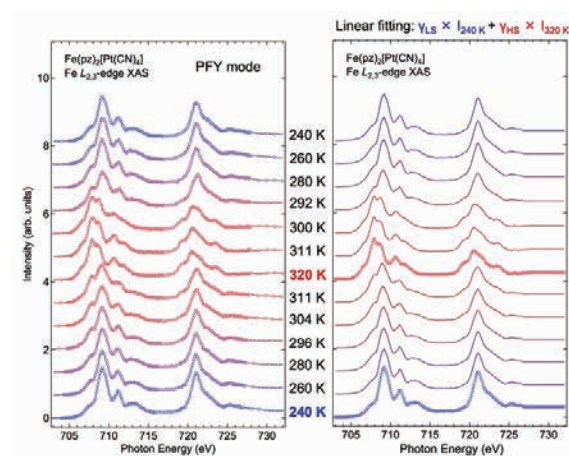


Fig. 1. The temperature dependent Fe  $L_{2,3}$ -edge XAS spectra and fitting analysis result of  $\text{Fe}(\text{pyrazine})_2[\text{Pt}(\text{CN})_4]$ .

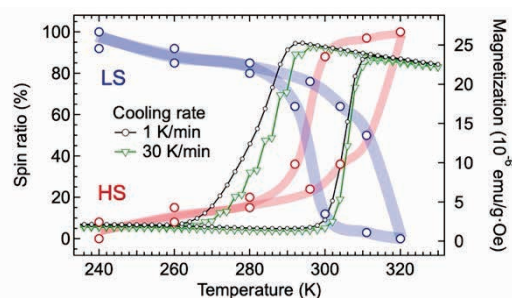


Fig. 2. The spin state weight of  $\text{Fe}^{2+}$  ions as the function of the temperature.

## Monitoring Phase Difference between Magnetic Substates in Helium Atom

T. Kaneyasu<sup>1,2</sup>, Y. Hikosaka<sup>3</sup>, M. Fujimoto<sup>2,4</sup>, H. Iwayama<sup>2,5</sup> and M. Katoh<sup>2,6</sup>

<sup>1</sup>SAGA Light Source, Tosu 841-0005, Japan

<sup>2</sup>Institute for Molecular Science, Okazaki 444-8585, Japan

<sup>3</sup>Institute of Liberal Arts and Sciences, University of Toyama, Toyama 930-0194, Japan

<sup>4</sup>Synchrotron Radiation Research Center, Nagoya University, Nagoya, 464-8603, Japan

<sup>5</sup>The Graduate University for Advanced Studies (SOKENDAI), Okazaki 444-8585, Japan

<sup>6</sup>Hiroshima Synchrotron Radiation Center, Hiroshima University, Higashi-Hiroshima 739-0046, Japan

Quantum manipulation of populations and reaction pathways in matter using the coherence properties of light, so-called coherent control, is currently one of the hottest research areas in optical physics and photochemistry. We have recently shown that synchrotron light is a new tool for achieving coherent control in the XUV and attosecond regimes [1–3]. This method is based on the use of the longitudinal coherence of individual light wave packets comprising incoherent radiation pulses. In all of these experiments, a pair of light wave packets was used to produce a pair of electron wave packets that interfere in a single atom. The quantum phase difference between the electron wave packets determines the behavior of the controlled (or probed) quantum state, and can be precisely controlled by varying the time delay between the light wave packets at the attosecond level. In this report, we present another approach to orbital alignment control of helium atoms [2] to monitor the phase difference between the interfering wave packets. The quantum phase difference between coherently excited magnetic substates is visualized as a quantum beat that appears in the fluorescence decay curve [4].

The experiment was performed at undulator beamline BLIU of the UVSOR-III synchrotron. A tandem undulator consisting of twin APPLE-II type variable polarization devices was operated in helical mode, providing pairs of 10-cycle left- and right-circularly polarized light wave packets. The central frequency of the fundamental radiation was set to about 24 eV. To measure the fluorescence decay curve of helium atoms, the UVSOR-III synchrotron was operated in the single bunch mode. The fluorescence photons emitted from helium atoms were detected by a photomultiplier tube. A magnetic field of approximately 20 G was applied parallel to the light propagation axis in the interaction region to induce Zeeman splitting between the magnetic substates of helium atoms.

Figure 1 shows fluorescence decay curves of  $1s6p$  excited state of helium atoms measured at eight different settings of the time delay  $\tau$  between the light wave packets. The quantum beat oscillations superimposed on the exponential decay with a lifetime of 13.1 ns are visible and the initial phases of the oscillations shift by varying the time delay. The

theoretical curves well reproduce the quantum beat structures observed in the measurement. Quantum beat measurement thus enables visualization of the quantum phase that has been used as a control knob for quantum manipulation of atomic systems

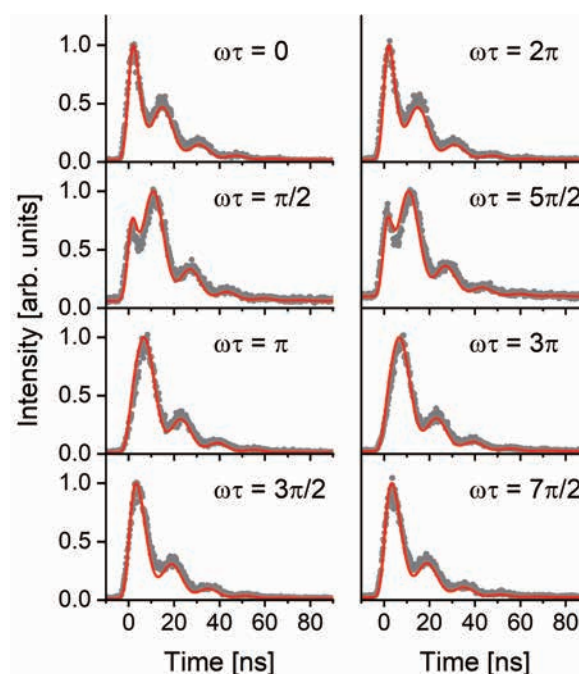


Fig. 1. Zeeman quantum beat in fluorescence decay of helium atoms [4]. The quantum phase  $\omega\tau$  is set to increase from 0 to  $7\pi/2$  with a step size of approximately  $\pi/2$  where  $\omega$  is the resonance frequency from the ground state to the  $1s6p$  state. The experimental data points are shown by gray circles and the red curves represent the calculation results

[1] Y. Hikosaka *et al.*, Nat. Commun. **10** (2019) 4988; *ibid.* **12** (2021) 3782.

[2] T. Kaneyasu *et al.*, Phys. Rev. Lett. **123** (2019) 233401.

[3] T. Kaneyasu *et al.*, Phys. Rev. Lett. **126** (2021) 113202.

[4] T. Kaneyasu *et al.*, J. Phys.: Conf. Ser. **2380** (2022) 012115.

BL1U

## High-Resolution Measurement of State-Resolved Photoelectron Circular Dichroism with Varied Photoionization Energies

H. Kohguchi<sup>1</sup>, Y. Hikosaka<sup>2</sup>, T. Kaneyasu<sup>3</sup>, S. Wada<sup>1</sup>, H. Ota<sup>4</sup>, M. Katoh<sup>1,4</sup> and Y-I. Suzuki<sup>5</sup>

<sup>1</sup>Graduate School of Advanced Science and Engineering, Hiroshima University,  
Higashi-Hiroshima 739-8526, Japan

<sup>2</sup>Institute of Liberal Arts and Sciences, University of Toyama, Toyama 930-0194, Japan

<sup>3</sup>SAGA Light Source, Tosu 841-0005, Japan

<sup>4</sup>UVSOR Synchrotron Facility, Institute for Molecular Science, Okazaki 444-8585, Japan

<sup>5</sup>School of Medical Technology, Health Sciences University of Hokkaido, Tobetsu, 061-0293, Japan

Measurements of photoelectron circular dichroism (PECD) require high-quality radiation for ionizing chiral molecules. One-photon photoionization in the vacuum ultraviolet region provides a fundamental understanding of the physical origin of PECD. Thus, we launched the PECD measurements at BL1U on February 2020. In the beginning of the feasibility test, the undulator conditions for circularly polarized light were optimized for a particular electron beam orbit, which was not used in regular beam time operation. In 2022, the normal electron beam orbit applicable to BL1U was developed so that the PECD measurements were possible in regular beam time. With the alternation of the electron beam orbit, the arrangement of the BL1U line was reformed.

We have employed a monochromator to reduce the spread of photon energy to measure the state-resolved PECD of chiral systems. The monochromator line with two mirror chambers is inserted between the BL1U port and our velocity-map imaging (VMI) apparatus (Fig. 1). We also modify the imaging device in this beam time. Our original setup used a resistive anode backed by an MCP detector to obtain the photoelectron images. We have replaced an imaging system consisting of a phosphor screen and a CCD camera with the anode type imager. The benefit of the optical camera system is real-time imaging during the measurement, which is expected to be advantageous in efficient searching for experimental conditions. Improved performance due to the renewal of the electron beam condition and the imaging system is evaluated in comparison with the previous PECD data [1].

We measured the PECD of methyl oxirane ( $\text{CH}_3\text{-C}_2\text{H}_3\text{O}$ ) in the new experimental setup. The PECD appears as asymmetric forward/backward intensity with respect to the circularly polarized light propagation. The result almost reproduced the previous data in that the forward-backward asymmetry (red/blue in Fig. 2) exhibited distinct state-dependence. The quality of the PECD data is the contrast of the forward/backward asymmetry, which is presented by blue/red contrast in the difference images of the right and left circular polarization in Fig. 2. The imaging system with the

camera provides an analog (Fig. 2(a)) and a counting (Fig. 2(b)) integration modes. The better PECD data was obtained by analog integration, although it is generally inferior to the counting mode in accuracy. This can be due to the too-slow counting integration of the software compared to the photoelectron counting rate. The renewal of the setup potentially improve our PECD measurements; however more detailed examination of several signal properties is necessary.

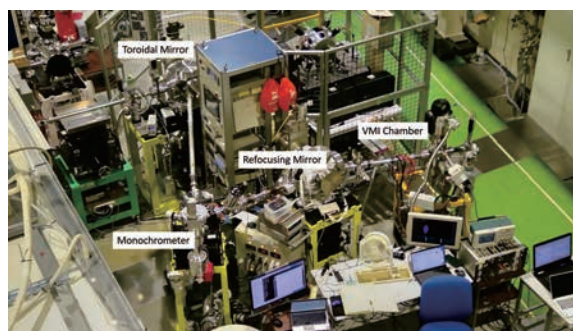


Fig. 1. New arrangement of the VMI apparatus for PECD measurements with a monochromator at the BL1U beamline.

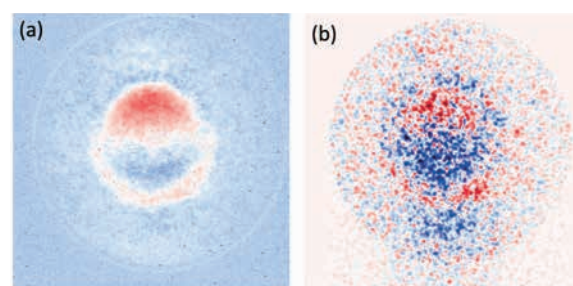


Fig. 2. Photoelectron circular dichroism (PECD) images of *s*-methyl oxirane measured with (a) analog integration mode and (b) counting integration mode. The propagation direction of the photoionization radiation is vertical in the figures.

[1] H. Kohguchi, Y. Hikosaka, T. Kaneyasu, S. Wada, H. Ota, M. Fujimoto, M. Kato and Y-I. Suzuki, UVSOR Activity Report **49** (2021) 106.

## M<sub>4,5</sub>-edge XANES Spectra of La and Nd Complex Oxides

H. Asakura<sup>1</sup>, M. Konno<sup>1</sup> and K. Nanakarage<sup>1</sup>

<sup>1</sup>Department of Applied Chemistry, Faculty of Science and Engineering, Kindai University, Kowakae, Higashiosaka, Osaka 577-8502, Japan

The areas of the pre-edge region at the lanthanide (Ln) L<sub>1</sub>-edge XANES spectra and the full with half maximum of the white line at the Ln L<sub>3</sub>-edge XANES spectra have been found to be good indicators of the local structure or symmetry of Ln elements in complex oxides [1-3]. However, it is usually difficult to obtain detailed electronic and/or geometric information of the Ln elements because of the inherent low energy resolution of Ln L-edge XANES spectra. Then, the M-edge XANES spectra, which are potentially much more sensitive to electronic structure, are employed to obtain more detailed information on the local structure. However, there are very few reports on the measurement of M-edge XANES spectra of Ln elements. In this study, we measured the M-edge XANES spectra of La or Nd complex oxides to investigate whether they can be used as indicators of local structure.

We prepared various La and Nd complex oxides by a polymerized complex method and confirmed that single phase polycrystalline powders were obtained by their XRD patterns. Nd M<sub>4,5</sub>-edge XANES spectra were obtained at BL2A, UVSOR using a Beryl double-crystal monochromator. We put each powder sample onto indium (In) foil bonded to the sample holder with carbon tape for total electron yield method measurement. To the best of our knowledge, there are no well-established data analysis procedure on the M-edge XANES spectra even for basic background removal or normalization. On the present data, we performed background removal in the pre-edge region below the M<sub>5</sub>-edge and normalization in the post-edge region above the M<sub>4</sub>-edge with Athena included in the Demeter package [4].

The Nd M<sub>4,5</sub>-edge XANES spectrum of Nd<sub>2</sub>O<sub>3</sub>, NdAlO<sub>3</sub>, NdMnO<sub>3</sub>, and Nd<sub>2</sub>CoO<sub>4</sub> was very similar to each other (Fig. 1), which indicated the oxidation state of Nd was the same, trivalent. By a closer look into the spectra, we found difference in relative absorbance at around 1006, 1008, and 1010 eV marked as peak A, B, and C at the Nd M<sub>4</sub>-edge XANES region (Fig. 2). The main contribution for the peak A and B is ascribed to the transition obeying the selection rule  $\Delta J = 0$ , and peak C is to  $\Delta J = -1$ , respectively [5]. In addition, theoretical simulation of Pr M<sub>4,5</sub>-edge XANES of Pr<sup>3+</sup>, [PrF<sub>6</sub>]<sup>3-</sup>, [PrCl<sub>6</sub>]<sup>3-</sup>, and [PrBr<sub>6</sub>]<sup>3-</sup> indicates possible sensitivity to the local structure of Pr [5]. However, at present, we do not have plausible interpretation of these characteristic features.

On the other hand, there are some questions as to whether the validity of the spectra can be guaranteed. For example, it is possible that differences due to

charge-up or slight variations in X-rays may be reflected into the spectra. In fact, on NdAlO<sub>3</sub>, significant difference was observed at another facility when the energy sweep direction was from the low energy to the high energy and from high to low, and the effect of charge-up was suspected. Thus, further careful study is needed.

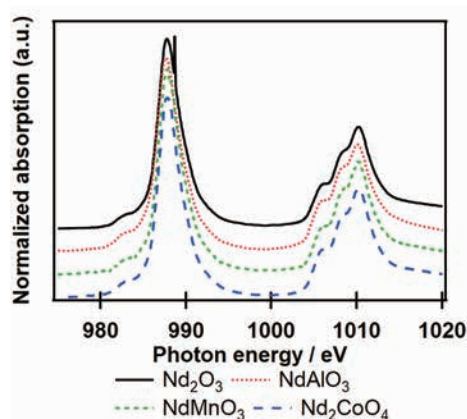


Fig. 1. Nd M<sub>4,5</sub>-edge XANES spectra of Nd complex oxides

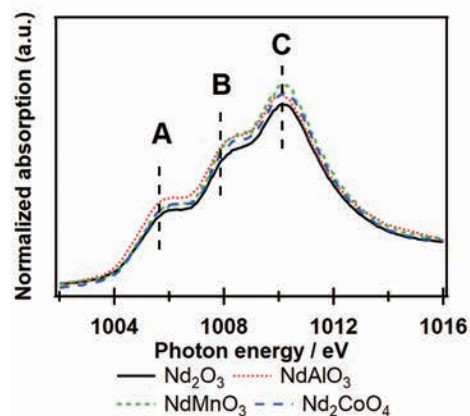


Fig. 2. Nd M<sub>4</sub>-edge XANES spectra of Nd complex oxides

- [1] H. Asakura *et al.*, *Inorg. Chem.* **53** (2015) 6048.
- [2] H. Asakura *et al.*, *J. Phys. Chem. C* **118** (2014) 20881.
- [3] H. Asakura *et al.*, *Inorg. Chem.* **60** (2021) 9359.
- [4] B. Ravel, M. Newville, *J. Synchrotron Rad.* **12** (2005) 537.
- [5] H. Ramanantoanina, *J. Chem. Phys.* **149** (2018) 054104.

BL3U

## O K-edge XAS of Photoreactions in Dissolved Oxygen on Lipid Bilayer

F. Kumaki<sup>1,2</sup>, M. Nagasaka<sup>3,4</sup>, Y. Kinjo<sup>5</sup>, R. Tero<sup>5</sup>, Y. Okano<sup>3</sup>, M. Fujimoto<sup>3,4</sup> and J. Adachi<sup>1,2</sup>

<sup>1</sup>Institute of Materials Structure Science, High Energy Accelerator Research Organization, Tsukuba 305-0801, Japan

<sup>2</sup>School of High Energy Accelerator Science, The Graduate University for Advanced Studies (SOKENDAI), Tsukuba 305-0801, Japan

<sup>3</sup>Institute for Molecular Science, Okazaki 444-8585, Japan

<sup>4</sup>School of Physical Sciences, The Graduate University for Advanced Studies (SOKENDAI), Okazaki 444-8585, Japan

<sup>5</sup>Toyohashi University of Technology, Toyohashi 441-8580, Japan

Porphyrim dyes form triplet states by the photoexcitation and relaxation process due to light absorption. Singlet oxygen ( $^1\text{O}_2$ ) is generated by the energy transfer from the triplet state of the porphyrin to the surrounding oxygen molecule with ground triplet state ( $^3\text{O}_2$ ). Singlet oxygen is highly reactive, and the generation of singlet oxygen by photosensitizers such as porphyrins is used for a cancer treatment as a photodynamic therapy [1]. The experimental research of the elementary processes of singlet oxygen production in a wet environment like in vivo conditions or in liquid is important for the development of chemistry and medicine.

From O K-edge X-ray absorption spectroscopy (XAS), we planned to measure the electronic state of singlet oxygen generated in solution directly via laser excitation of photosensitizers. We have recently developed and demonstrated the time-resolved XAS system for optical reactions in liquid samples by a synchronizing synchrotron radiation pulse and a laser pulse at KEK Photon Factory [2]. At the UVSOR, we have been developed a similar time-resolved XAS system by synchronizing soft X-ray pulses (530 eV, 128 ps) and visible laser pulses (400 nm). Since the lifetime of singlet oxygen in liquid is  $\sim 3 \mu\text{s}$  [3], the synchrotron radiation pulse whose pulse duration is about 100 ps, is suitable to observe its dynamics. In this report, the change of XAS spectra between the ground state and the state under laser irradiation was measured.

The O K-edge XAS spectra were measured by using the liquid flow cell at BL3U. The liquid cell consists of a liquid layer sandwiched between two  $\text{Si}_3\text{N}_4$  membranes on which lipid bilayers were prepared. The buffer solution (NaCl 100 mM, HEPES 25 mM) bubbled with oxygen gas was continuously pumped into the cell at a flow rate of 100  $\mu\text{l/hr}$  to keep the dissolved oxygen on the lipid bilayer. The emphasized peak of dissolved oxygen on the lipid bilayers can be measured by thinning the liquid layer to the limit [4].

For the formation of singlet oxygen with a photoreaction, the chlorophyll-*a* was used as a photosensitizer and was added to the lipid bilayer. By irradiating the visible laser (400 nm, 0.5mW) which is second order harmonic generation (SHG) of Ti:sapphire laser to the cell, the chlorophyll-*a* was photoexcited.

We attempted to observe singlet oxygen produced from dissolved oxygen by the energy transfer from the triplet state of chlorophyll-*a* caused by the photoexcitation and the relaxation process. The O K-edge XAS spectra of dissolved oxygen in the ground state and during laser irradiation were compared, and the difference was observed.

Figure 1 shows the O K-edge XAS spectra of lipid bilayer. The peak around 531 eV is assigned as dissolved oxygen molecules adsorbed on lipid bilayers. The spectrum of the state during laser irradiation (laser on) shows the lower photon energy shift compared to that in the ground state (laser off). We will discuss the formation mechanism of singlet oxygen from the difference spectrum with the help of the inner-shell calculations.

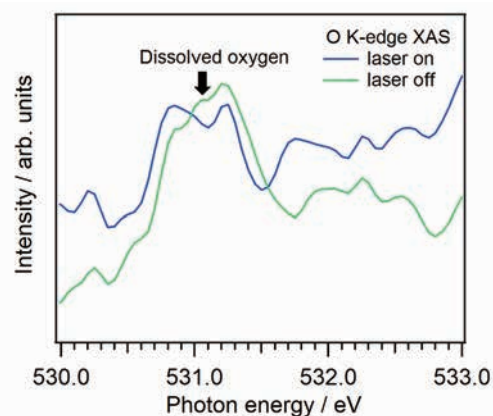


Fig. 1. O K-edge XAS spectra of dissolved oxygen, whose peak positions are around 531 eV, on lipid bilayers. The green and blue lines are the ground state (laser off) and the state under laser irradiation (laser on), respectively.

- [1] M. Ethirajan *et al.*, *Chem. Soc. Rev.* **40** (2011) 340.
- [2] F. Kumaki *et al.*, *J. Chem. Phys.* **158** (2023) 104201.
- [3] C. A. Long and D. R. Kearns, *J. Am. Chem. Soc.* **97** (1975) 2018.
- [4] F. Kumaki *et al.*, *UVSOR Activity Report*, **49** (2022) 118.

## Carbon K-edge X-ray Absorption Spectra of Liquid Ethanol Reproduced by Quantum Chemical Calculations and Molecular Dynamics Simulations

M. Nagasaka<sup>1,2</sup>

<sup>1</sup>*Institute for Molecular Science, Okazaki 444-8585, Japan*

<sup>2</sup>*The Graduate University for Advanced Studies (SOKENDAI), Okazaki 444-8585, Japan*

Liquid ethanol (EtOH) shows complicated liquid structures with the continuous formation and decay of hydrogen bond networks including the hydrophobic interactions between ethyl groups. Soft X-ray absorption spectroscopy (XAS) has potential to investigate the structures of liquid EtOH separating the contributions of the hydrogen bond interactions and hydrophobic interactions between ethyl groups. Recently, we have measured C K-edge XAS of liquid EtOH by using a transmitted-type liquid cell [1]. However, the inner-shell spectra of the model structures did not reproduce the spectral shapes of liquid EtOH since the liquid structures reconfigured continuously. In this study, we have performed C K-edge inner-shell calculations of liquid EtOH by the summation of the calculated spectra of excited EtOH molecules with neighbor molecules extracted from the liquid structures obtained by the molecular dynamics (MD) simulations [2].

MD simulations of liquid EtOH were conducted by using the program package GROMACS [3]. The equilibrium structure including one thousand EtOH molecules were obtained after a simulation time of 101 ns at 25 °C and 1 atm in the isobaric-isothermal ensemble. The inner-shell calculations were conducted by using the program package GSCF3 [4]. The ground and core excited states were calculated within the Hartree-Fock method, namely,  $\Delta$ SCF (self-consistent field). As shown in the inset of Fig. 1, we have extracted one thousand small liquid structures that consist of excited EtOH molecules and neighbor EtOH molecules within the  $\text{CH}_2$ - $\text{CH}_2$  distance of 6 Å from the excited EtOH molecules. The inner-shell spectrum of liquid EtOH was obtained by the summation of one thousand calculated spectra of small liquid structures.

Figure 1(a) shows the experimentally obtained C K-edge XAS spectrum of liquid EtOH [1]. The spectrum shows four peaks: The peak at 287.311 eV is the transition of the  $\text{CH}_3$  C 1s electron to the 3s-type Rydberg orbital ( $\text{CH}_3$  3s). The peaks at 288.025 eV and 288.760 eV are assigned as the transition of the  $\text{CH}_3$  C 1s electron to the 3p-type Rydberg orbitals ( $\text{CH}_3$  3p1 and 3p2). The peak at 289.710 eV is assigned to the transition of the  $\text{CH}_2$  C 1s electron to the 3s-type Rydberg orbital ( $\text{CH}_2$  3s). Figure 1(b) shows the calculated inner-shell spectrum of liquid EtOH from the summation of one thousand calculated spectra of small liquid structures. The calculated spectra well reproduced four Rydberg peaks and spectra shapes

obtained by the experiments. However, the calculated higher energy shifts from gas to liquid phases are overestimated compared to the experimental values. It is because the induced polarization of the surrounding EtOH molecules above the  $\text{CH}_2$ - $\text{CH}_2$  distance of 6 Å is ignored, which causes the lower energy shifts of the XAS peaks. We have also calculated C K-edge inner-shell spectra of liquid methanol and confirmed that the calculated spectra well reproduced the experimental results [5].

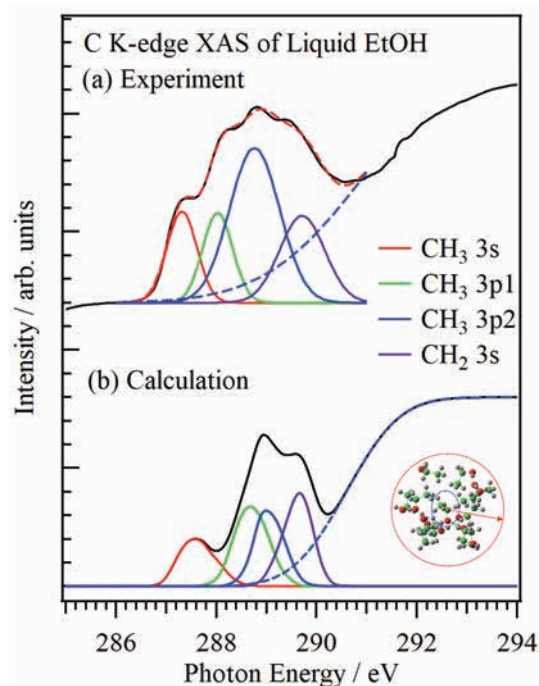


Fig. 1. C K-edge XAS spectra of liquid EtOH from (a) experiments and (b) calculations. The inset shows one of the liquid structures used for the inner-shell calculations, where EtOH molecules were extracted from the liquid structure within the  $\text{CH}_2$ - $\text{CH}_2$  distance of 6 Å from the central EtOH molecule.

- [1] M. Nagasaka *et al.*, *J. Phys. Chem. B* **126** (2022) 4948.
- [2] M. Nagasaka, *J. Chem. Phys.* **158** (2023) 024501.
- [3] M. J. Abraham *et al.*, *SoftwareX* **1-2** (2015) 19.
- [4] N. Kosugi, *Theor. Chim. Acta* **72** (1987) 149.
- [5] M. Nagasaka *et al.*, *J. Phys. Chem. B* **118** (2014) 4388.

BL3U

## Observation of the Behavior of Sumanene in Organic Solvents by C K-edge XAS Experiment

Y. Uetake<sup>1,2</sup>, K. Sugimura<sup>1</sup>, R. Ihsan<sup>1</sup>, M. Nagasaka<sup>3</sup> and H. Sakurai<sup>1,2</sup>

<sup>1</sup>Division of Applied Chemistry, Graduate School of Engineering, Osaka University, Suita 565-0871, Japan

<sup>2</sup>Innovative Catalysis Science Division, Institute for Open and Transdisciplinary Research Initiatives (ICS-OTRI), Osaka University, Suita, 565-0871, Japan

<sup>3</sup>Institute for Molecular Science, Okazaki 444-8585, Japan

Sumanene, a bowl-shaped  $\pi$ -extended molecule, has been found to exhibit a unique columnar packing structure in the crystalline state due to the intermolecular CH- $\pi$  interactions between them[1]. Such interactions are expected to occur in the solution state. Previously, our group reported the infrared spectroscopy of sumanene in *para*-H<sub>2</sub> matrix. However, there are still few reports on the dynamic behavior of  $\pi$ -conjugated molecule, including sumanene, in solution state. In this study, we performed solution-phase X-ray absorption spectroscopy (XAS) of  $\pi$ -extended molecules to investigate dynamic behavior, such as intermolecular interactions, in organic solvents.

The solution-phase C K-edge XAS experiments were performed at soft X-ray beamline BL3U using a transmission-type liquid flow cell[2]. Sumanene (**1**), corannulene (**2**), and triphenylene (**3**) were dissolved in tetrahydrofuran, respectively, to give sample solutions (10 mmol/L). The thus-prepared solution was injected to the cell by syringe. After adjusting the optical path length by controlling helium pressure, XAS experiment was conducted.

Fig. 1 shows C K-edge XAS data of sumanene, corannulene, and triphenylene, respectively. In the case of sumanene, relatively sharp peak was observed at 285.2 eV, which is assigned as the transition of C 1s electron to C=C  $\pi^*$  orbitals. Meanwhile, two peaks were observed at 284.8 and 285.3 eV. This result indicated the difference of the electronic structure between sumanene and corannulene. Inner-shell calculations were performed using GSCF3 program[3,4] and it was found that the simulated peak pattern was matched with experimental spectra in the case of sumanene and corannulene, although these calculations did not reproduce the relative energy value (Fig. 2). From this calculation, it was found that the peak at 284.8 eV corresponds to the internal carbons of corannulene. Interestingly, XAS data for triphenylene showed two split peaks, unlike the case of sumanene. Since the inner-shell calculations of sumanene and corannulene exhibited almost the same spectral shape, the spectroscopic difference is thought to represent the difference in the behavior in solution.

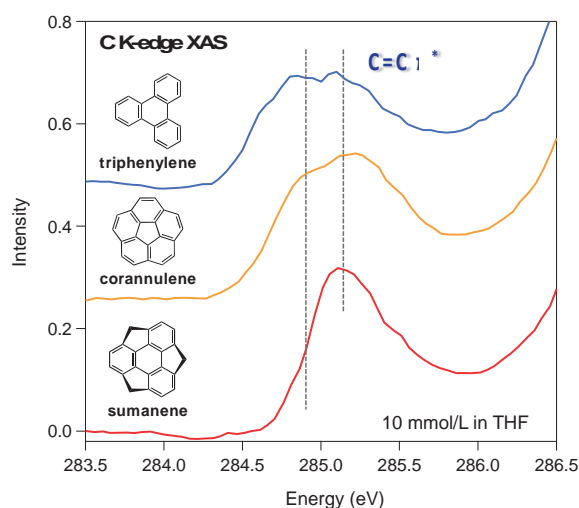


Fig. 1. C K-edge XAS data of sumanene, corannulene, and triphenylene.

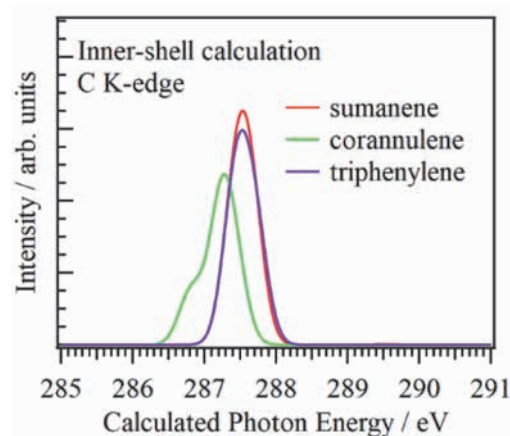


Fig. 2. Inner-shell calculations of sumanene, corannulene, and triphenylene.

[1] H. Sakurai, T. Daiko, H. Sakane, T. Amaya and T. Hirao, *J. Am. Chem. Soc.* **127** (2005) 11580.

[2] M. Nagasaka and N. Kosugi, *Chem. Lett.* **50** (2021) 956.

[3] N. Kosugi and H. Kuroda, *Chem. Phys. Lett.* **74** (1980) 490.

[4] N. Kosugi, *Theor. Chim. Acta* **72** (1987) 149.

## Operando Observation of Adsorbed Anions on the Surface of Nickel Catalysts by Soft X-ray Absorption Spectroscopy

A. Sakai<sup>1</sup>, Z. Li<sup>1</sup>, K. Harada<sup>1</sup>, S. Tsunekawa<sup>1</sup>, M. Nagasaka<sup>2</sup> and M. Yoshida<sup>1,3</sup>

<sup>1</sup>Yamaguchi University, Tokiwadai, Ube, Yamaguchi 755-8611, Japan

<sup>2</sup>Institute for Molecular Science, Myodaiji, Okazaki 444-8585, Japan

<sup>3</sup>Blue Energy Center for SGE Technology (BEST), Ube, Yamaguchi 755-8611, Japan

Recently, electrochemical hydrogen production from water has been attracting attention to develop a sustainable society. In this system, nickel oxides electrodeposited in carbon electrolyte solution are known to be one of the efficient electrocatalyst for oxygen production [1-2]. Thus, various operando spectroscopic analyses have applied to the nickel catalysts in order to reveal the physical properties and functions. However, the role of carbonate anion in the electrolyte solution is still not fully understood. From this background, in this study, the role of adsorbed carbonate anion was investigated for the nickel electrocatalysts by X-ray absorption fine structure (XAFS) measurements using hard X-ray and soft X-ray under operando conditions.

The handmade electrochemical cell was used with a Pt wire counter electrode and an Ag/AgCl reference electrode (NaCl). The nickel electrocatalysts were prepared by electrodeposition on Au thin film in a solution containing Ni<sup>2+</sup> and carbonate anion (Ni-C<sub>i</sub> catalyst). The operando Ni K-edge XAFS were carried out by fluorescence mode in the SPring-8 BL01B1, and the operando C K-edge XAFS were performed by transmission mode at BL3U in the UVSOR synchrotron.

First, SEM, EDX, UV-vis and XPS measurements were also measured to investigate the surface morphology and chemical states of electrodeposited catalysts. Next, we tested the electrochemical activity of oxygen evolution reaction (OER), suggesting that the prepared Ni-C<sub>i</sub> functioned as highly efficient OER electrocatalyst. Moreover, the electrolyte solution was exchanged from potassium carbonate solution (K-C<sub>i</sub>) to potassium phosphoric solution (K-P<sub>i</sub>) during monitoring the OER activity, indicating that the water splitting activity of the Ni-C<sub>i</sub> catalyst was preserved in the K-P<sub>i</sub> electrolyte solution.

The operando Ni K-edge XAFS measurements were performed to investigate the electronic state and local structure of the Ni-C<sub>i</sub> catalyst. The result of EXAFS analysis showed that the peaks of Ni-O and Ni-Ni bonds were observed at similar positions compared to the  $\gamma$ -NiOOH reference sample, suggesting that the local structure of Ni in the catalyst was consistent with that of  $\gamma$ -NiOOH. Moreover, the local structure of the catalyst in the K-P<sub>i</sub> solution was also maintained that of  $\gamma$ -NiOOH.

Finally, the operando C K-edge XAFS measurements were carried out for the Ni-C<sub>i</sub> catalyst under the catalytic reaction (Fig. 1). The result showed that carbonate anions were adsorbed on the catalyst surface. The adsorbed peak was remained even after exchanging the electrolyte solution from K-C<sub>i</sub> to K-P<sub>i</sub>. Thus, this result suggests that the carbonate anions are strongly adsorbed on the Ni-C<sub>i</sub> catalyst. The adsorbed carbonate anions are likely to contribute to stabilize the  $\gamma$ -NiOOH structure with high oxidation number Ni. On the basis of these discussions, we concluded that the  $\gamma$ -NiOOH structure stabilized by adsorbed carbonate anions could efficiently decompose water molecule to oxygen gas due to the high oxidation number Ni of active site.

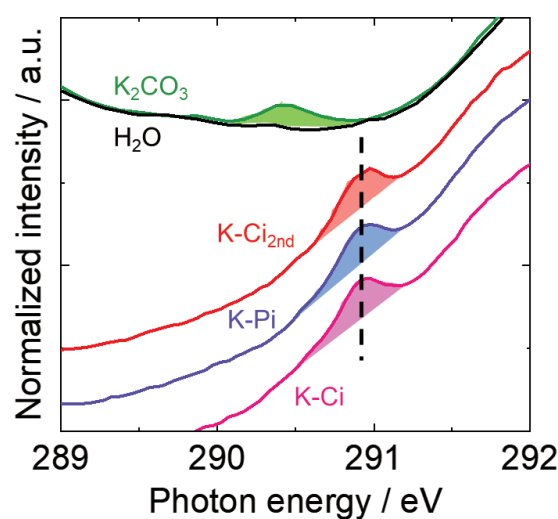


Fig. 1. Operando C-K edge XAFS spectra for Ni-C<sub>i</sub> electrocatalyst with exchanging the electrolyte solution between K-C<sub>i</sub> and K-P<sub>i</sub> by transmission mode at BL3U in the UVSOR synchrotron. The electrolyte aqueous solution of potassium carbonate was measured as reference compounds.

- [1] K. S. Joya, Y. F. Joya, and H. J. M. de Groot, *Adv. Energy Mater.*, **4** (9) (2014) 1301929.
- [2] T. Shinagawa, M. T. Ng and K. Takanahe, *Angew. Chem. Int. Ed. Eng.*, **56** (18) (2017) 5061.
- [3] A. C. Garcia, T. Touzalin, C. Nieuwland, N. Perini and M. T. M. Koper, *Angew. Chem. Int. Ed. Eng.*, **58** (37) (2019) 12999.

BL3U

## Temperature Effects on the X-ray Absorption Spectrum of Aqueous $\text{Ca}(\text{NO}_3)_2$ Recorded at the Ca $L$ -edge

D. Céolin<sup>1</sup>, T. Saisopa<sup>2</sup>, Y. Rattanachai<sup>2</sup>, H. Yuzawa<sup>3</sup> and N. Kosugi<sup>3</sup>

<sup>1</sup>Synchrotron SOLEIL, l'Orme des Merisiers, Saint-Aubin, F-91192 Gif-sur-Yvette Cedex, France

<sup>2</sup>Department of Applied Physics, Faculty of Sciences and Liberal Arts, Rajamangala University of Technology Isan, Nakhon Ratchasima 30000, Thailand

<sup>3</sup>UVSOR Synchrotron Facility, Institute for Molecular Science, Okazaki 444-8585, Japan

Calcium dication is frequently studied due to its abundance in human body and its importance in biological processes. Thus, its local structure determination is the subject of number of investigations, both experimental (XRD, EXAFS, MD, etc.) and theoretical (QM/MM, MD). In aqueous solutions, X-ray absorption spectroscopy (XAS) was used to probe the effect of the concentration on e.g., the hydration number, but the influence of the temperature was not investigated, despite some information was reported on other techniques [1].

In this context, we performed XAS measurements at the BL3U beamline on aqueous  $\text{Ca}(\text{NO}_3)_2 \cdot 4\text{H}_2\text{O}$ , using the liquid cell in transmission mode. The setup offers the possibility to monitor its temperature (T). We choose a high concentration close to the solubility limit of this salt in water at 0°C, that is 1050 g/L. The results are presented in the Figure 1. Each spectrum has its background removed.

A full attribution of the different structures was given in a previous paper [2]. The  $2p^{-1}$  spin-orbit contributions are located below (above)  $\sim 351$  eV for  $L_3$  ( $L_2$ ), respectively. The temperature change from 0 to 60°C do not influence the splitting between the two main lines, nor the position of the smaller peaks. The intensity ratio between peaks 1 and 2, which gives information on the crystal field 10Dq value, is small. Despite we observe a slight modification of this ratio with T, we consider it as not relevant as it does not follow the T variation and is attributed to the background removal procedure.

A more precise analysis shows a slight blue-shift of the right side of the peaks toward the high photon energies following the temperature increase (see insert in Fig. 1 corresponding to a zoom of the main  $L_3$  line), whereas the low energy sides remain quasi-unchanged. The width of peak 1 for each T is shown in Fig. 2. The photon bandwidth and the detector contribution are constant and lead to an experimental resolution of 166 meV, whereas the Lorentzian broadening contribution shows a slight increase roughly from 200 to 250 meV within the T going from 0 to 60°C.

Temperature effects were already probed by XAS in electrolyte aqueous solutions at the O K-edge. For a 5 M LiCl aqueous solution [3], a redshift of the pre-edge resonance maximum was observed when T increases. It was attributed to the change of the distance between the

bulk water molecules with T, whereas molecules in the first hydration shell of lithium ion are more strongly bonded to it and less sensitive to T variations. In the present case, the sample concentration is high and close to the solubility limit at 0°C. We can argue that thermal motion at low T is reduced and slightly increases in this T range. These observations should be confirmed by complementary measurements.

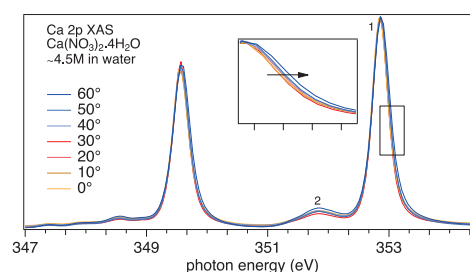


Fig. 1. X-ray absorption spectra of a 4.5 M  $\text{Ca}(\text{NO}_3)_2 \cdot 4(\text{H}_2\text{O})$  aqueous solution, recorded in the vicinity of the Ca  $2p$  ionization threshold, for temperatures in the 0-60°C range.

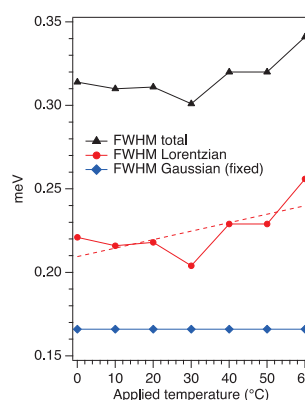


Fig. 2. Influence of temperature on the width of the main line (full width at half maximum: FWHM). The Gaussian and Lorentzian contributions are extracted.

[1] A. A. Zavitsas, *J. Phys. Chem. B*, **109** (2005) 20636.

[2] T. Saisopa *et al.*, *J. Electron Spectrosc. Relat. Phenom.*, **244** (2020) 146984.

[3] M. Nagasaka *et al.*, *J. Phys. Chem. B*, **121** (2017) 10957.

## Self-Assembled Hierarchical Nanosegregated Chiral Intermediate Phases Composed of Two Different Achiral Bent-Core Molecules

F. Araoka<sup>1</sup>, Y. Takanishi<sup>2</sup>, S-W. Choi<sup>3</sup> and H. Iwayama<sup>4,5</sup>

<sup>1</sup>RIKEN Center for Emergent Matter Science (CEMS), Wako, Saitama 351-0198, Japan

<sup>2</sup>Faculty of Science, Kyoto University, Sakyo, Kyoto 606-8502, Japan

<sup>3</sup>Department of Advanced Materials Engineering for Information and Electronics, Kyung Hee University, Yongin 17104, Republic of Korea

<sup>4</sup>UVSOR Synchrotron Facility, Institute for Molecular Science, Okazaki, Aichi 444-8585, Japan

<sup>5</sup>School of Physical Sciences, The Graduate University for Advanced Studies (SOKENDAI), Okazaki, Aichi 444-8585, Japan

Chirality is fascinating because of its fundamental importance in nature. As we presented in the activity report of the previous year, achiral BC molecules are well-known for spontaneous chiral resolution at the macroscopic scale despite the chiral-carbon-atom-free (hence, achiral) molecules (Fig. 1a). The so-called B4 phase—often the lowest temperature phase of BCs—is one such chiral mesophase in which a helical nanofilament superstructure is spontaneously self-assembled. In this case, structural chirality, observed as helical handedness, originates from the layered chirality of tilted smectic layers twisting along the filaments. Another very similar type of chiral phase formed by achiral bent-core molecules is the dark conglomerate (DC) phase. The DC also exhibits optically resolved domains with strong optical activity, but it looks more isotropic. The fundamental morphology of DCs comprises disordered sponge-like structures of tilted smectic layers. Although sponge-like structures do not have morphological chirality, it is understood that the observed macroscopic optical activity is attributed to the layered chirality of the tilted smectic layers.

Recently, we explored some interesting chirality-related phenomena in nano-separated intermediate phases composed of two achiral bent-core liquid crystalline molecules, one of which is circularly polarized luminescence (CPL) in the nano-separated intermediate phase blended with a luminescent dye [1]. Following up this work, we further extended this concept to realize dual-chiral intermediate phase (as illustrated in the right panel of Fig. 1a) of coexisting B4 and DC phases, using nanophase segregation between two bent-core molecules and hierarchical self-organization. Interestingly, the luminescence dissymmetry factor of CPL from the nano-separated dual-chiral phase of the B4 and DC was one order of magnitude higher than that of the previously reported chiral phases of the bent-core system [2].

Thus, the present dual-chiral phase system looks promising. However, its structure has not yet been confirmed. Since the system is consisting of two mesophases, direct observation methods such as using transmission electron microscope aren't usable.

Therefore, for this sake, we performed resonant soft X-ray scattering (RSoXS) experiment to identify the nano-separated phases. Our RSoXS setup was prepared in BL3U of UVSOR at IMS – A homemade vacuum chamber equipped with a cooled CCD camera (Newton, Andor) was used for small angle detection ( $2\theta \sim 1\text{--}15^\circ$ ). In the present study, the X-ray photon energy was chosen as 284.5 eV, corresponding to the carbon K-edge absorption of the present sample mixtures. The sample mixture was sandwiched between two SiN membrane films and then sealed not to exposed to vacuum. The sample chamber also equips a furnace to heat up the sample.

The RSoXS profile of the dual chiral phase (Fig. 1b) was compared with those of the only-B4 (Fig. 1c) and only-DC (Fig. 1d) phases. The RSoXS result clearly shows that the patterns of two chiral phases are superimposed in the dual chiral phase. In addition, we carefully examined the dual chiral phase with circular dichroism spectroscopy, polarizing light microscopy, and differential scanning calorimetry, we concluded that the model proposed in Fig. 1a is reasonable in the present dual chiral system.

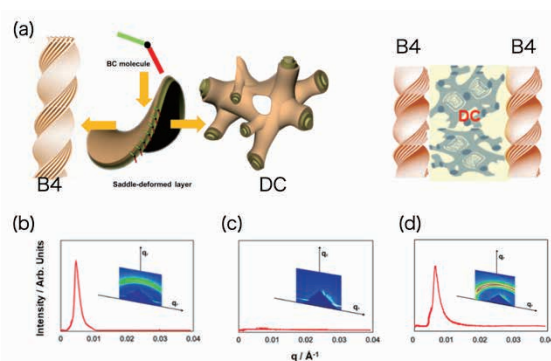


Fig. 1. (a) Schematics of the nanoscopic structures of the B4 and DC phases, and the nano-separated dual chiral phase. (b, c, d) RSoXS patterns obtained for (b) B4, (c) DC, and (d) dual chiral phases. [2]

[1] Kim *et al. Adv. Funct. Mater.* **29** (2019) 1903246.

[2] Lee *et al. Int. J. Mol. Sci.* **23** (2022) 14629.

BL3U

## X-ray Absorption Spectra of Metal Carbonyl Solutions

T. Sasaki and H Xu

Department of Complexity Science and Engineering, Graduate School of Frontier Sciences,  
The University of Tokyo, Kashiwa 277-8561, Japan

XAS measurements for liquid samples have been enabled at UVSOR BL3U, giving new insights for physicochemical properties of materials [1]. We have studied O-K edge XAS measurements for cellobiose aqueous solutions and found that XAS signals can be simulated with CP2K and hydrogen bonding with water molecules affect the relative intensity of XAS peaks. In this study metal carbonyl solutions were examined for XAS measurements to gain information of metal carbonyls dissolved in liquid phase, since metal carbonyls can be regarded as good models for both homogeneous and heterogeneous catalysts. Therefore we can expect XAS method will act as a new characterization tool for chemical and catalytic processes in liquid phase. In this study  $\text{Mo}(\text{CO})_6$  and  $\text{Ru}_3(\text{CO})_{12}$  were chosen as target molecules.

XAS measurements for liquid samples were conducted at UVSOR BL3U using facilities developed by Nagasaka et al. [1]. The liquid sample cell with  $\text{Si}_3\text{N}_4$  membranes was adopted, where the thickness of the liquid layer was controlled by the He gas pressure around the cell.

Fig. 1 shows O-K XAS spectrum for  $\text{Mo}(\text{CO})_6$  (40 mg) in 10 ml  $\text{CH}_3\text{CN}$  at room temperature. Concentration is 15 mM. This condition is close to the saturated solution. A sharp peak at 531.25 eV was observed and can be attributed to excitation to  $\text{C}=\text{O}$   $1\pi^*$  level. Broad features above 534 eV can be associated with sigma bonding of C-O ligand.

Fig. 2 shows O-K XAS spectrum for  $\text{Ru}_3(\text{CO})_{12}$  (3 mg) in 5 ml  $\text{CHCl}_3$  at room temperature. Concentration is 0.94 mM. This condition is also close to the saturated solution. It is noticed that peak intensity for Fig. 2 is weaker than that for Fig. 1, because of the low solubility of  $\text{Ru}_3(\text{CO})_{12}$ . A peak was found at 531.65 eV and can be attributed to excitation to  $\text{C}=\text{O}$   $1\pi^*$  level. Broad features above 534 eV can be associated with sigma bonding of C-O ligand.

Due to the limitation of rather low concentration C-K edge measurements are difficult since overlap with absorption peaks by solvent molecules affect the peaks associated with CO ligand.

For the precise peak assignments MD calculation for carbonyl species dissolved in solvent molecules and

core excitation simulation are now in progress. It is expected to conduct measurements of other metal carbonyls and observation of ligand exchange. Whether site discrimination, for example atop coordination and bridging coordination is possible or not is also interesting point to be clarified.

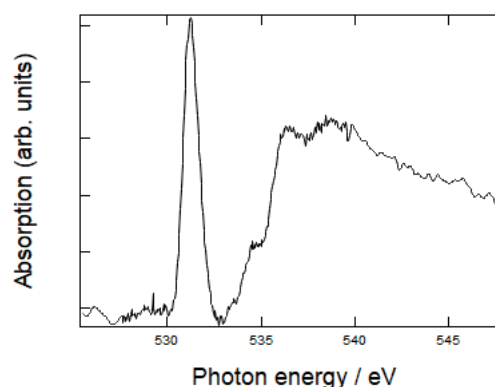


Fig. 1. O-K XAS spectrum for  $\text{Mo}(\text{CO})_6$  (40 mg) in 10 ml  $\text{CH}_3\text{CN}$  at room temperature.

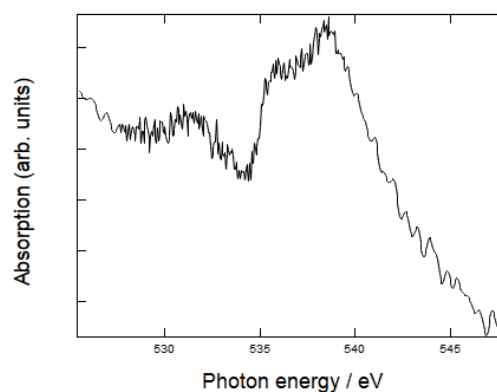


Fig. 2. O-K XAS spectrum for  $\text{Ru}_3(\text{CO})_{12}$  (5 mg) in 5 ml  $\text{CHCl}_3$  at room temperature.

[1] M. Nagasaka *et al.*, *J. Electrosc. Relat. Phenom.* **200** (2015) 293.

[2] D. Akazawa *et al.*, *J. Chem. Phys.* **156** (2022) 044202.

## Soft X-ray Absorption of Photocatalysts for Artificial Photosynthesis: Ultraviolet Light Irradiation in Water

H. Onishi<sup>1,2</sup>, Yi Hao Chew<sup>1</sup>, K. Matsui<sup>1</sup>, N. Ichikuni<sup>3</sup> and T. Yoshida<sup>4</sup>

<sup>1</sup>*School of Science, Kobe University, Kobe 657-8501, Japan*

<sup>2</sup>*Division of Advanced Molecular Science, Institute for Molecular Science, Okazaki 444-8585, Japan*

<sup>3</sup>*Graduate School of Engineering, Chiba University, Chiba 263-8522, Japan*

<sup>4</sup>*Reserch Center for Artificial Photosynthesis, Osaka Metropolitan University, Osaka 558-8585, Japan*

Sodium tantalate ( $\text{NaTaO}_3$ ) and strontium titanate ( $\text{SrTiO}_3$ ) provide a class of semiconductor photocatalysts which produce hydrogen–oxygen mixed bubbles in the overall water splitting reaction, when properly doped with metal cations [1, 2]. We are conducting a series of studies to answer the question of why doping with metal cations raised the quantum yield of the reaction [3]. Here, soft X-ray absorption is applied for characterizing the electronic structure of the photocatalysts in the presence and absence of ultraviolet (UV) light for bandgap excitation.

$\text{NaTaO}_3$  particles doped with Sr cations (2 mol%) were prepared through a solid-state reaction, and characterized with EDX and XRD in Kobe University. The particles were suspended with water ( $5 \text{ g l}^{-1}$ ) and sent to a liquid film cell for transmission absorption by a syringe pump (Figure 1). To avoid sedimentation of the particles, pH of the suspension was tuned at 13, far from isoelectric point of the particles.

An Hg–Xe lamp (200 W) was used to irradiate UV light for photocatalyst excitation. The photodiode detecting transmitted X-ray was capped with a nickel filter to minimize stray UV light from the lamp and higher-order X-ray passing through the monochromator.

Figure 2 shows an oxygen K edge absorption spectrum of Sr-doped  $\text{NaTaO}_3$  photocatalyst particles suspended in water. It was not straightforward to place a significant amount of the photocatalyst particles in the water film pinched with two SiN membranes. An

absorption band appeared at 531.5 eV was ascribed to the photocatalyst particles but to be further examined, since the oxidized layer of the membranes may provide an absorption band at 530–531 eV.

Purin Sathirathai, an undergraduate student of Sirindhorn International Institute of Technology, Thammasat University in Thailand, assisted us in photocatalyst preparation under Sakura Science Exchange Program by Japan Science and Technology Agency. This study was supported by JSPS KAKENHI (grant numbers 18KK0161 and 22H00344).

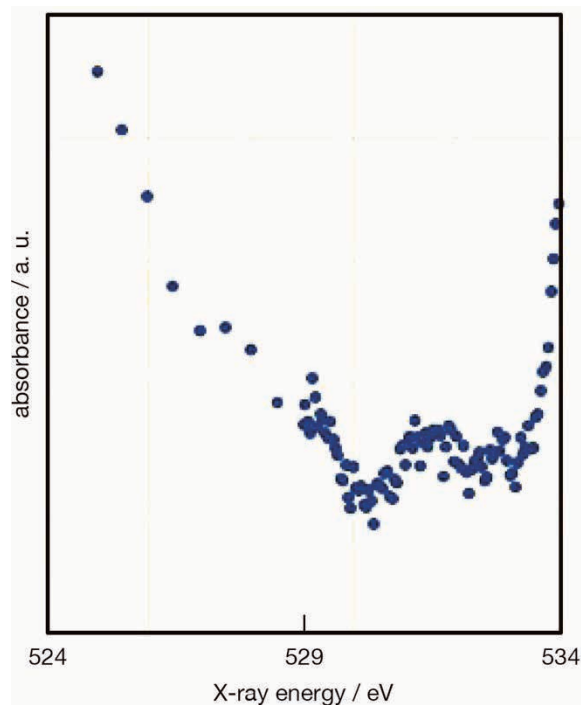


Fig. 2. Oxygen K edge absorption spectrum of  $\text{NaTaO}_3$  photocatalyst particles doped with Sr cations observed in water without UV light irradiation. The absorbance spectrum is shown in an arbitrary unit as a function of X-ray energy.



Fig. 1. Strontium-doped  $\text{NaTaO}_3$  photocatalyst particles suspended in water. White suspension in the syringe was sent to the liquid film cell for transmission XAFS measurements.

[1] H. Kato, K. Asakura, A. Kudo, *J. Am. Chem. Soc.* **125** (2003) 3082.

[2] T. Takata, J. Jiang, Y. Sakata, M. Nakabayashi, N. Shibata, V. Nandal, K. Seki, T. Hisatomi, K. Domen, *Nature* **581** (2020) 411.

[3] H. Onishi, *ChemSusChem* **12** (2019) 1825.

BL3U

## Hydration of Dimethyl Sulfoxide Probed by Liquid-Phase Soft X-ray Absorption Spectroscopy

C. Sugahara<sup>1</sup>, K. Okada<sup>1</sup> and H. Iwayama<sup>2,3</sup>

<sup>1</sup>Graduate School of Advanced Science and Engineering, Hiroshima University,  
Higashi-Hiroshima 739-8526, Japan

<sup>2</sup>Institute for Molecular Science, Okazaki 444-8585, Japan

<sup>3</sup>School of Physical Sciences, The Graduate University for Advanced Studies (SOKENDAI),  
Okazaki 444-8585, Japan

Soft X-ray absorption spectroscopy offers information on the local atomic environment of a molecular system under study by the resonant excitation of the local site. Different characters of water in solution, i.e. bulk and hydrated water, can be detected by the spectroscopy. The subtle differences in character, however, prevent us from clear distinction from one another without a useful analysis method. We have proposed a new quantity, called the excess absorption coefficient, for the analysis of absorption spectra of solutions and applied to the acetone–water binary system [1]. The analysis gives a successful extraction of the hydrated component.

This study is intended for generalization by the application of the method to another solution. The system of interest for this purpose is dimethyl sulfoxide (DMSO) aqueous solution. The DMSO molecule is more polarized than acetone. This is shown by the difference in the values of excess molar enthalpy. The acetone–water mixture has negative values only in the dilute region [2], while the DMSO–water mixture has negative values at all fractions and has greater absolute values [3]. We expect that more intensity in the absorption component of hydrated water for the latter mixture.

The experiments were performed on the soft X-ray beamline, BL3U. The photoabsorption spectra were measured in the oxygen K-edge region, with sample cell windows made of silicon nitride with a thickness of 150 nm. The incident photon energy was calibrated to the peak at 530.88 eV of a polymer film [4]. The absorption coefficient was evaluated so as to match the value at 547.85 eV to that tabulated in the database [5]. The sample solutions were prepared by mixing liquid DMSO with purified water to give the molar fraction of DMSO,  $x_D$ , in the range 0–0.35.

Observed absorption spectra of DMSO aqueous solutions are shown in Fig. 1. The spectrum for pure DMSO ( $x_D = 1$ ) has peaks at 532.6 and 534.0 eV. The former peak, assigned to the  $\pi^* \leftarrow O\ 1s$  transition of DMSO, is clearly dependent on  $x_D$ . The  $4a_1 \leftarrow O\ 1s$  absorption peak of water at 534.7 eV seems to shift to lower energies with  $x_D$ . The behavior is, however, not conclusive due to the overlap with the hump at about

534 eV which is assigned to another resonance transition of DMSO. This fact indicates that in this system the distinction of hydrated water from the bulk water requires a physicochemical analysis method: The system is a perfect system for testing our method of analysis. The results of the analysis will be published elsewhere.

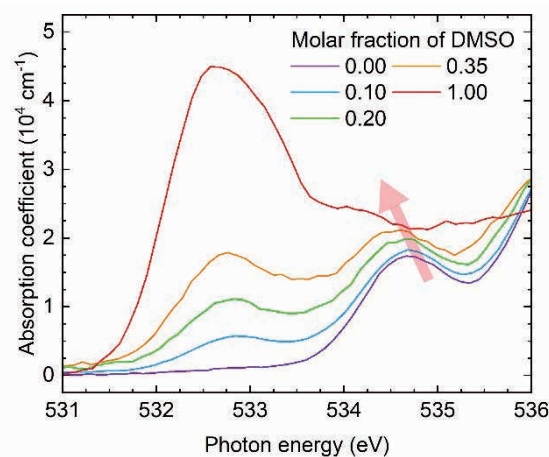


Fig. 1. The soft X-ray absorption spectra of liquid water and DMSO aqueous solutions measured for a series of molar fractions of DMSO. The spectrum of the liquid DMSO is also shown for comparison.

- [1] K. Okada, C. Sugahara, H. Iwayama and M. Nagasaka, *UVSOR Activity Report 2021*, **49** (2022) 117.
- [2] B. Löwen and S. Schulz, *Thermochim. Acta* **262** (1995) 69.
- [3] T. Kimura and S. Takagi, *Netsu Sokutei* **13** (1986) 2.
- [4] M. Nagasaka, H. Yuzawa, T. Horigome and N. Kosugi, *J. Elec. Spectrosc. Relat. Phenom.* **224** (2018) 93.
- [5] C. T. Chantler *et al.*, NIST Standard Reference Database 66 (1995; last update in 2005), available at <https://www.nist.gov/pml/x-ray-form-factor-attenuation-and-scattering-tables>.

## Multielectron-ion Coincidence Spectroscopy of I 4d inner-shell Photoionization of CH<sub>3</sub>I and CH<sub>2</sub>I<sub>2</sub> Molecules

M. Fushitani<sup>1</sup>, Y. Hikosaka<sup>2</sup> and A. Hishikawa<sup>1,3</sup>

<sup>1</sup>Graduate School of Science, Nagoya University, Furo-cho, Chikusa, Nagoya, Aichi, 464-8602, Japan

<sup>2</sup>Institute of Liberal Arts and Sciences, University of Toyama, 2630 Sugitani, Toyama, Toyama, 930-0194, Japan

<sup>3</sup>Research Center for Materials Science, Nagoya University, Furo-cho, Chikusa, Nagoya, Aichi, 464-8602, Japan

Inner-shell photoionization of molecules often leads to formation of highly charged states followed by fragmentation processes. Identifying which ion species are generated from which electronic states is of great importance for the basic understanding of ultrafast processes associated with inner-shell ionization. Among others, multielectron-ion coincidence spectroscopy using a magnetic bottle type electron spectrometer is a powerful approach to obtain such information [1-3]. Here, we applied it to I 4d inner-shell ionization of CH<sub>3</sub>I and CH<sub>2</sub>I<sub>2</sub> molecules to investigate fragmentation processes occurring from doubly charged states.

Electrons generated by photoionization with a synchrotron radiation at 100 eV were guided from the interaction region into a time-of-flight (TOF) tube (1.5 m) by magnetic fields from a permanent magnet and solenoid coil while ions were pushed into the tube by applying pulsed voltages to ion-collecting electrodes [1]. These electrons and ions were detected by a microchannel plate placed on the opposite side of the TOF tube.

Figure 1 shows Auger electron spectra obtained in coincidence with I 4d photoelectrons, I<sup>+</sup> ions and selected counterpart ions for (a) CH<sub>3</sub>I and (b) CH<sub>2</sub>I<sub>2</sub>. These Auger peaks provide information on the location of excited electronic states producing the fragment ion pairs. In Fig.1(a), the pair of I<sup>+</sup> and CH<sub>3</sub><sup>+</sup> ions are mainly generated together with Auger electrons having kinetic energies around 20-30 eV which correspond to doubly charged states associated with outer-valence configurations [4,5]. On the other hand, Auger signals are observed below 20 eV for the (I<sup>+</sup>, CH<sub>2</sub><sup>+</sup>), (I<sup>+</sup>, CH<sup>+</sup>), and (I<sup>+</sup>, C<sup>+</sup>) ion pairs, showing that these ion pairs are formed preferentially from higher excited states related to inner-valence configurations [4].

In the case of CH<sub>2</sub>I<sub>2</sub> (Fig.1(b)), the (I<sup>+</sup>, CH<sub>n</sub>I<sup>+</sup>) ion pair reflecting the single C-I bond cleavage is produced mostly with Auger electrons having 25-32 eV kinetic energies. By contrast, Auger signals appear in the lower energy region for other ion pairs associated with two C-I bond fissions, indicating the dissociations occur in excited doubly charged states.

The present study shows a promising approach for applications and fundamental understanding of nonlinear inner-shell ionization of iodine-containing molecules by intense free-electron lasers.

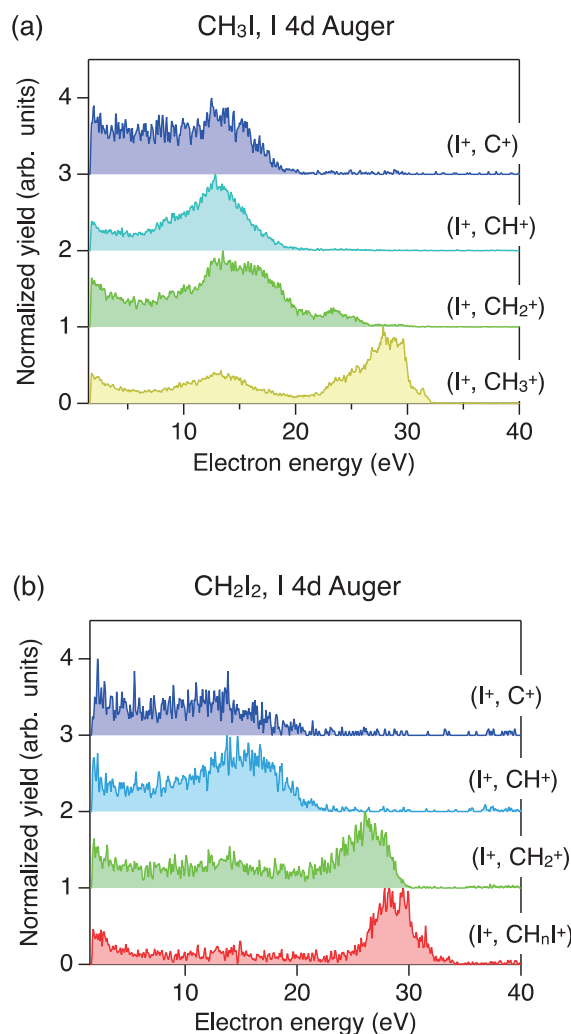


Fig. 1. PEPEPIPICO spectra of I 4d inner-shell photoionization at 100 eV for (a) CH<sub>3</sub>I and (b) CH<sub>2</sub>I<sub>2</sub>.

[1] Y. Hikosaka, *J. Electron Spectrosc. Rel. Phenom.* **255** (2022) 147158.

[2] Y. Hikosaka and E. Shigemasa, *Int. J. Mass Spectrom.* **439** (2019) 13.

[3] M. Fushitani *et al.*, *Phys. Rev. A (Letter)* **107** (2023) L021101.

[4] A. Hult Roos *et al.*, *Chem. Phys.* **491** (2017) 42.

[5] A. Bodi *et al.*, *Phys. Chem. Chem. Phys.* **25** (2023) 7383.

BL4B

## Quadruple Auger Decay from Xe 4s Core-Hole State Studied by Multi-Electron-Ion Coincidence Spectroscopy

Y. Hikosaka

*Institute of Liberal Arts and Sciences, University of Toyama, Toyama 930-0194, Japan*

Emissions of multiple Auger electrons, following inner-shell photoionization of atoms in the soft X-ray region, can occur within the permitted limits of the energetics. Multi-electron coincidence spectroscopy using a magnetic bottle electron spectrometer is a powerful means for studying multiple Auger decay. Discrimination of multiple Auger processes against dominant single Auger decay can be improved by filtering multi-electron coincidences with the additional detection of product ions relevant to the multiple Auger processes. By adding such ion detection capability to a magnetic bottle electron spectrometer, multi-electron-ion coincidence measurements can be performed very efficiently [1-3].

In this study, quadruple Auger decay of the Xe 4s core-hole state is investigated by multi-electron-ion coincidence spectroscopy with a magnetic bottle electron spectrometer [4]. Figure 1(a) shows the total electron spectrum (black curve) and the spectrum filtered by coincidence with  $\text{Xe}^{5+}$  ions (red curve), where the 4s photoelectron peak is observed around a kinetic energy of 180 eV. From the net intensities of the 4s peaks observed in the total and coincidence spectra, the fraction of the quadruple Auger path in the 4s decay was determined to be 16%.

The two-dimensional map in Fig. 1(b) displays the correlation between the fastest electron's energy and the sum of the energies of the other four electrons, determined from the six-fold coincidence including  $\text{Xe}^{5+}$  ion. It is possible to recognize structures running diagonally. The diagonal structures correspond to the formation of  $\text{Xe}^{5+}$  levels, resulting from the energy conservation (photon energy) - (binding energy of the  $\text{Xe}^{5+}$  state) = (fastest electron's energy) + (the sum of the energies of the other four electrons). Enhancement of  $\text{Xe}^{5+}$  formation is observed at the 4s photoelectron energy, corresponding to quadruple Auger decay from the  $4s^{-1}$  state.

Figure 2 shows the  $\text{Xe}^{5+}$  distribution populated by the quadruple Auger decay from the  $4s^{-1}$  state. The distribution is obtained by integrating the coincidence counts in Fig. 1(b) along the direction (fastest electron's energy) + (the sum of the energies of the other four electrons) = const., where the fastest electrons were restricted to be of the 4s photoelectron energy range. In addition to the formation of the  $5p^{-5}$  levels, both histograms show substantial formation of excited  $\text{Xe}^{5+}$  levels. The final formation fractions of the  $5p^{-5}$ ,  $5s^{-1}5p^{-4}$ , and  $5s^{-2}5p^{-3}$  levels by the quadruple Auger decay are estimated to be 7%, 7% and 2% of the 4s decay, respectively.

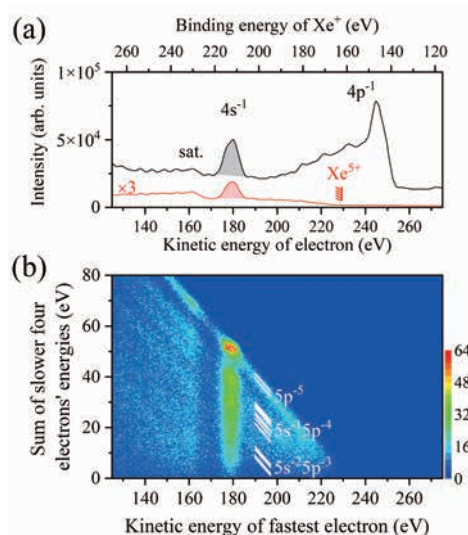


Fig. 1. (a) Inner shell photoelectron spectra of Xe observed at a photon energy of 391.7 eV, obtained for total events in the coincidence dataset (black) or by filtering with the detection of a  $\text{Xe}^{5+}$  ion (red). (b) Two-dimensional map showing the correlation between the fastest electron's energy and the sum of the energies of the other four electrons.

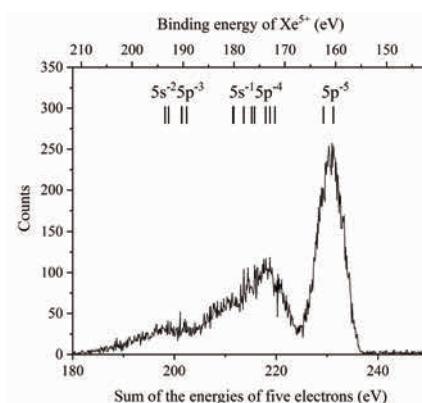


Fig. 2.  $\text{Xe}^{5+}$  distribution populated by the quadruple Auger decay from the  $4s^{-1}$  state.

- [1] Y. Hikosaka and E. Shigemasa, *Int. J. Mass Spectrom.* **439** (2019) 13.
- [2] Y. Hikosaka, *J. Electron Spectrosc. Relat. Phenom.* **255** (2022) 147158.
- [3] Y. Hikosaka and S. Fritzsche, *Phys. Chem. Chem. Phys.* **24**, (2022) 17535.
- [4] Y. Hikosaka, *Phys. Rev. A* **106** (2022) 062814.

## Metastable $\text{OCS}^{3+}$ States Investigated by Multi-Electron–Ion Coincidence Spectroscopy

Y. Hikosaka

*Institute of Liberal Arts and Sciences, University of Toyama, Toyama 930-0194, Japan*

Triply charged molecular ions are always energetically unstable due to Coulomb repulsion between the three positive charges. However, low-lying trication states in some limited molecules are known to be stable for more than  $\mu\text{s}$  due to the presence of deep minima on the potential energy surfaces. In this study, metastability of  $\text{OCS}^{3+}$  states populated by the S 2p double Auger decay has been investigated by multi-electron–ion coincidence spectroscopy. A magnetic bottle electron spectrometer with ion detection capability [1-4] was employed for this investigation, and the high detection efficiencies for electrons enabled to derive the information of stability of  $\text{OCS}^{3+}$  electronic states.

The double Auger decay of the  $\text{S}2\text{p}^{-1}$  states in OCS can be isolated by inspecting electron triple coincidences including a S2p photoelectron. The two-dimensional map in Fig. 1 is derived from the electron triple coincidences, displaying the energy correlation between the two electrons other than the S2p photoelectron. On this map, several diagonal stripes are identified in (faster electron's energy) + (slower electron's energy) = 95–115 eV, which are formed by double Auger decay. The population of the  $\text{OCS}^{3+}$  states formed by the S2p double Auger decay is revealed by projecting the coincidence yields on the diagonal axis of (faster electron's energy) = (slower electron's energy). The resultant  $\text{OCS}^{3+}$  spectrum is shown in Fig. 2 as black curve. Several peaks are observed in the kinetic energy range of 95–115 eV, corresponding to the diagonal structures seen on the two-dimensional map in Fig. 1. Moreover, a broad structure is seen in the binding energy range of 80–95 eV. These spectral profiles agree with the previous investigation by Eland et al. [5].

Metastability of  $\text{OCS}^{3+}$  states can be investigated by inspecting the ion species detected in further coincidence with S2p photoelectron and two Auger electrons. The double Auger spectrum filtered by further coincidence with parent  $\text{OCS}^{3+}$  ion is presented in Fig. 2 as red shaded spectrum. Only the peak for the ground  $3\pi^{-3}{}^2\Pi$  state at a binding energy of 60 eV is exhibited in the spectrum, revealing that the ground state is metastable in the  $\mu\text{s}$  regime. An MRCI/CASSCF calculation [5] predicts the ground  $3\pi^{-3}{}^2\Pi$  state has a potential surface with a potential well along both directions lengthening the CS and CO bonds, although excited  $\text{OCS}^{3+}$  states are all unbound to lengthening the

CS bond. The present observation is in consistent with the calculation results.

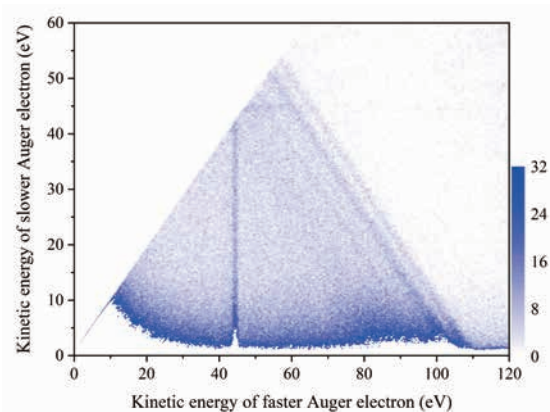


Fig. 1. Two-dimensional map showing the energy correlations between two Auger electrons emitted in the S 2p double Auger decay of OCS, which was derived from electron triple coincidence.

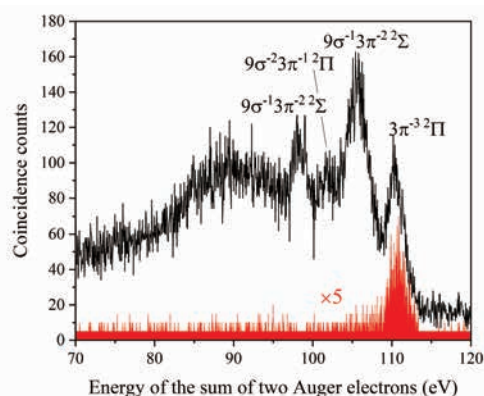


Fig. 2.  $\text{OCS}^{3+}$  spectra formed by the S2p double Auger decay of OCS: total spectrum (black solid curve) and the one filtered with further coincidence with parent  $\text{OCS}^{3+}$  ions (red shaded spectrum).

- [1] Y. Hikosaka and E. Shigemasa, *Int. J. Mass Spectrom.* **439** (2019) 13.
- [2] Y. Hikosaka, *J. Electron Spectrosc. Relat. Phenom.* **255** (2022) 147158.
- [3] Y. Hikosaka and S. Fritzsche, *Phys. Chem. Chem. Phys.* **24**, (2022) 17535.
- [4] Y. Hikosaka, *Phys. Rev. A* **106** (2022) 062814.
- [5] J.H.D. Eland et. al, *J. Chem. Phys.* **132** (2010) 014311.

BL4B

## Soft X-ray Absorption Study of Semiconductor Photocatalysts for Highly Efficient Oxidation of Water

T. Yoshida<sup>1</sup>, N. Ichikuni<sup>2</sup>, H. Onishi<sup>3,4</sup> and Yi Hao Chew<sup>3</sup>

<sup>1</sup>Reserch Center for Artificial Photosynthesis, Osaka Metropolitan University, Osaka 558-8585, Japan

<sup>2</sup>Graduate School of Engineering, Chiba University, Chiba 263-8522, Japan

<sup>3</sup>School of Science, Kobe University, Kobe 657-8501, Japan

<sup>4</sup>Division of Advanced Molecular Science, Institute for Molecular Science, Okazaki 444-8585, Japan

A number of metal oxides including gallium oxide, ( $\text{Ga}_2\text{O}_3$ ), sodium tantalate ( $\text{NaTaO}_3$ ) and strontium titanate ( $\text{SrTiO}_3$ ) provide a class of semiconductor photocatalysts highly efficient for the overall water splitting reaction, when properly doped with foreign metal cations. [1-3]. We are conducting a series of studies to answer the question of why metal-cation doping raised the quantum yield of the reaction [4]. Here, soft X-ray absorption is applied for characterizing the electronic structure of the photocatalysts in the presence and absence of ultraviolet (UV) light for bandgap excitation.

Sub-micrometer-sized  $\text{Ga}_2\text{O}_3$  particles were prepared in Osaka Metropolitan University, while  $\text{NaTaO}_3$  doped with  $\text{Sr}^{2+}$  cations and  $\text{SrTiO}_3$  doped with  $\text{Al}^{3+}$  cations were prepared in Kobe University. Oxygen K edge absorption spectrum of the photocatalysts particles was observed under vacuum in the presence and absence of UV light provided by a Hg–Xe lamp (200 W).

In XAFS measurement of oxygen K edge, the photocatalyst particles were molded as disks of 7-mm diameter. The disks were placed in a vacuum chamber, irradiated with incident X-ray, and fluorescent X-ray was detected with a silicon drift detector (SDD). The detector was capped with a 150-nm-thick aluminum film (LUXEL, TF110) to minimize contribution of stray UV light to detector response (Fig. 1).

Figure 2 shows a set of oxygen K edge spectra observed on Sr-doped  $\text{NaTaO}_3$  photocatalyst disk. The low energy band, which was assigned to the electronic transition from the oxygen 1s to oxygen 2p levels hybridized with tantalum 5d orbitals, appeared at 531.2

eV in the absence of UV light irradiation. The band shifted by 0.4 eV to the low-energy side under UV irradiation.

A possible reason of the band shift is the conduction band partially filled with bandgap-excited electrons. The density of vacant states, the final states of the K edge absorption, should have modified with the electrons excited from the valence band. The oxidation state of Ta cations decreased from 5+ to 4+ by the bandgap excitation.

This study was supported by JSPS KAKENHI (grant numbers 18KK0161 and 22H00344).

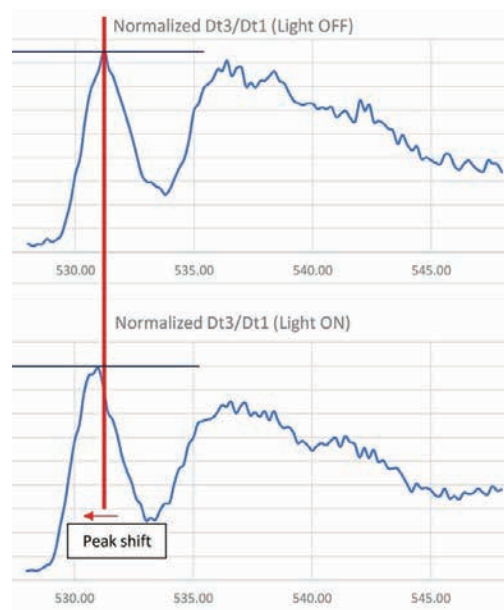


Fig. 2. Oxygen K edge absorption spectrum of a Sr-doped  $\text{NaTaO}_3$  photocatalyst disk in the absence (upper panel) and presence (lower panel) of UV-light irradiation.

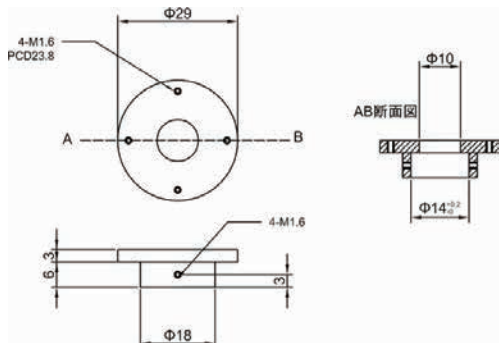


Fig. 1. A devise capping the SDD with the aluminum filter for fluorescence yield detection of oxygen K edge absorption spectrum under UV-light irradiation.

[1] Y. Sakata, T. Hayashi, R. Yasunaga, N. Yanaga, H. Imamura, *Chem. Commun.* **51** (2015) 12935.

[2] H. Kato, K. Asakura, A. Kudo, *J. Am. Chem. Soc.* **125** (2003) 3082.

[3] T. Takata, J. Jiang, Y. Sakata, M. Nakabayashi, N. Shibata, V. Nandal, K. Seki, T. Hisatomi, K. Domen, *Nature* **581** (2020) 411.

[4] H. Onishi, *ChemSusChem* **12** (2019) 1825.

## High-Resolution Photoelectron Spectroscopy of Unexplored Chiral Systems for Demonstration of the Photoelectron Circular Dichroism

H. Kohguchi<sup>1</sup>, Y. Hikosaka<sup>2</sup>, T. Kaneyasu<sup>3</sup>, S. Wada<sup>1</sup> and Y-I. Suzuki<sup>4</sup>

<sup>1</sup>Graduate School of Advanced Science and Engineering, Hiroshima University,  
Higashi-Hiroshima 739-8526, Japan

<sup>2</sup>Institute of Liberal Arts and Sciences, University of Toyama, Toyama 930-0194, Japan

<sup>3</sup>SAGA Light Source, Tosu 841-0005, Japan

<sup>4</sup>School of Medical Technology, Health Sciences University of Hokkaido, Tobetsu, 061-0293, Japan

Photoelectron circular dichroism (PECD) has attracted attention as a novel molecular chirality detection method. One of the remarkable attributes of PECD is that the asymmetric photoelectron angular distribution is generated from isotropically oriented molecules in the gas phase. In addition, PECD depends on the final ionic states so that the PECD data can be related to the chirality of the molecular orbitals. We have been conducting state-resolved PECD measurements with the UVSOR BL1U beam line. Although the circularly polarized light supplied by the BL1U undulator is indispensable for detecting the state-dependence of PECD [1], the narrower photon energy spread is desired for resolving the electronic structure of the observed photoelectron spectra. The width of the experimental photoelectron spectra is limited by our VMI apparatus as well as the light source. High-resolution photoelectron spectra provide unambiguous assignment of the electronic states which is applicable to the PECD image data. For combining the narrow band spectra with the PECD results measured in BL1U, we have developed the VMI apparatus and inspected the performance in the BL7B beam line.

We adopt two types of imaging systems in our VMI apparatus employs: a resistive anode and a CCD camera. The total resolution was evaluated in measurement of Ar photoelectron images in BL7B. The photoelectron images measured with the resistive anode imager exhibited sufficiently high resolution that the spin-orbit dual ring was resolved, as shown in Fig. 1 (a)-(d). The same measurement with the camera system yielded the image data with a comparable resolution but with a poor signal-to-noise ratio (Fig. 1 (A)-(D)). This is because the numerical operation determining the photoelectron positions of the camera system was found to be less efficient by 10 % of the resistive anode imager. The performance of these two imaging systems was directly examined with the narrow band light source, providing necessary improvement toward the state-resolved PECD measurements.

The photoionization experiments of chiral compounds with a heat nozzle were conducted as another evaluation of the machine developments. An increase of the photoelectron in a particular photon energy region was

measured with the elevated nozzle temperature, which was ascribed to the vaporized chiral molecules (Fig. 2). The photoelectron emitted in the shorter wavelength than 100 nm was regarded to be due to contaminated water, which is generally hard to eliminate. This result indicates that the density of the vapor in the irradiation volume needed to be increased for the state-resolved PECD measurements of new chiral systems. The machine developments should be reconsidered based on the results of the BL7B measurements.

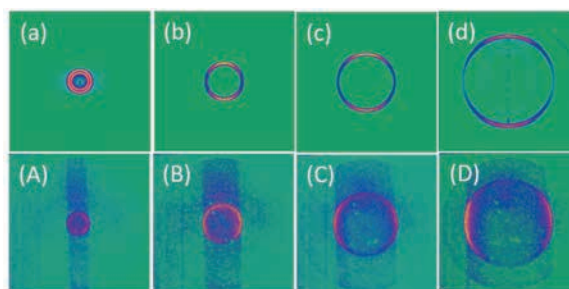


Fig. 1. Photoelectron images of Ar measured at various photon energy from 75 nm to 50 nm; (a)-(d) with a resistive anode imager, (A)-(D) with a CCD camera capturing a phosphor screen image.

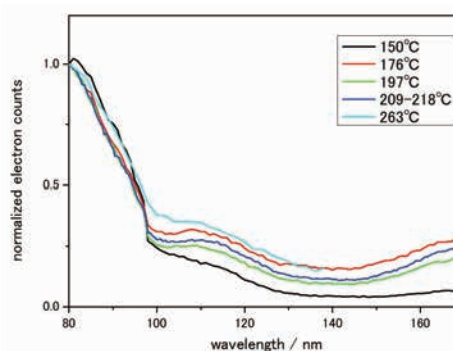


Fig. 2. Photoelectron yield spectrum of binaphthol at various nozzle temperatures near the ionization threshold.

[1] H. Kohguchi, Y. Hikosaka, T. Kaneyasu, S. Wada, H. Ota, M. Fujimoto, M. Kato and Y-I. Suzuki, UVSOR Activity Report **48** (2020) 93.

BL7B

## The Challenge of Photoionization Plasma Generation Using Synchrotron Radiation Source for Study of Plasmas in Interstellar Space and in Nuclear Fusion Devices

M. Kobayashi<sup>1</sup>, H. Iwayama<sup>2</sup>, J. Takahashi<sup>3</sup>, S. Yoshimura<sup>1</sup>, H. Ota<sup>2</sup>, K. Kobayashi<sup>3</sup>,  
M. Katoh<sup>2,4</sup>, H. Nakamura<sup>1</sup>, I. Sakon<sup>5</sup>, K. Sawada<sup>6</sup> and Y. Kebukawa<sup>3</sup>

<sup>1</sup>National Institute for Fusion Science, 322-6 Oroshi-cho, Toki 509-5292, Japan

<sup>2</sup>UVSOR Synchrotron Facility, Institute for Molecular Science, Myodaiji, Okazaki 444-8585, Japan

<sup>3</sup>Yokohama National University, 79-5 Tokiwadai, Hodogaya-ku, Yokohama 240-8501, Japan

<sup>4</sup>Hiroshima Synchrotron Radiation Center, Hiroshima University, 739-0046, Japan

<sup>5</sup>Department of Astronomy, Graduate School of Science, University of Tokyo, Tokyo 113-0033, Japan

<sup>6</sup>Graduate School of Engineering, Shinshu University, Nagano, Japan

An interstellar space is filled with interstellar plasmas, which is generated by ionization by cosmic rays or by interstellar radiation field [1]. In nuclear fusion devices [2], it is considered that neutral atoms and molecules in the divertor region are photoionized by a light coming from the confinement region and the scrap-off layers, where hot plasmas emit light in various energy ranges, from EUV through visible to infrared ranges. Characteristics and roles of the photoionized plasmas are, however, not yet fully understood: What is the dependency of the density and temperature of the photoionized plasmas on the energy range of the light? How the plasma transport under an influence of space magnetic field affects chemical evolution of organic molecules in the interstellar space? How the photoionization process affects the atomic/molecular processes in the divertor region of the nuclear fusion devices, which plays important roles on a device wall heat load mitigation?

To address these issues, we attempt to generate photoionized plasmas by using the Synchrotron Radiation Source UVSOR-III. There has been substantial works on the photoionization by using laser light with relatively high power source. In the present work, however, we are interested in photoionization by the radiation field (continuum light) in order to mimic the interstellar radiation field and the radiation in the fusion devices, such as Bremsstrahlung. It is expected that the photoionization by the continuum light is significantly different from those by the laser, because of the continuous energy distribution that can excite and ionize at various energy levels simultaneously.

The beamline BL7B is used to generate a continuum light from 30 to 400 nm with 0th order emission. A gas cell has been installed inside the irradiation chamber to maintain high pressure of the sample gas while keeping a good vacuum condition for the beamline. A high gas pressure is necessary to enhance the photoionization events through an interaction between the photons and neutral atoms/molecules. Fig.1 shows the gas cell based on a ICF34 cube. Holes of diameter of 1 to 2 mm are made for the injection of the light into the cell as well as for a gas outlet. Optical fibers are installed at the gas

cell for measurements of spectra of VUV, visible and mid infrared range from the photoionized plasmas. The gas is fed to the cell through the pipe at the top of the cell. An electrode is situated at the bottom of the cell and is biased up to +30V with respect to the ground to measure electron saturation currents of the plasmas.

As a sample gas, Ar and hydrogen were introduced respectively. The ionization potentials of the gaseous are 14.5 and 13.6 eV, respectively. The light from the BL7B beamline has a peak intensity at around 50 nm, which corresponds to a photon energy of 24.8 eV. The gas pressure inside the gas cell could be increased to an order of 1 Pa while the ambient pressure outside of the cell was kept at an order of  $10^{-4}$  Pa and the pressure at the upstream of the beamline was at an order of  $10^{-6}$  Pa.

A beam of a few mm diameter could be injected into the gas cell through the holes. The photon flux of the beam was measured with a photodiode, and was estimated at an order of  $10^{11}$  photons/s/mm<sup>2</sup>. However, no significant signal of photoionization was obtained this time. More challenges to come by optimizing the gas cell shape and the measurement system.

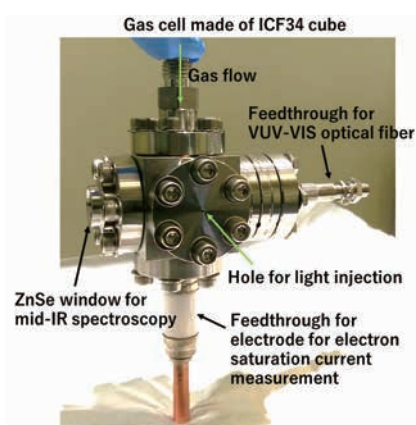


Fig. 1. A gas cell for the photoionization experiments.

[1] E.F.van Dishoeck *et al.*, *Faraday Discuss* **133** (2006) 231.

[2] M. Kobayashi *et al.*, *Nucl. Fusion* **62** (2022) 056006.

# UVSOR User 6

